Numerical investigation of water droplet dynamics in a low-temperature fuel cell microchannel: Effect of channel geometry

Xun Zhu [a,*], Qiang Liao [a], P.C. Sui [b], Ned Djilali [b]

[a] *Institute of Engineering Thermophysics, Chongqing University, Chongqing 400044, China*
[b] *Institute for Integrated Energy Systems, and Department of Mechanical Engineering, University of Victoria, Victoria, BC V8W 3P6, Canada*

ARTICLE INFO

ABSTRACT

The sensitivity of liquid water to geometry of cathode gas microchannel in low-temperature fuel cells is investigated numerically. The two-phase flow is resolved using 3D CFD simulations with the volume-of-fluid (VOF) method. Simulations for microchannels with different cross-sections, including rectangle with aspect ratios in a range of 0.1–2, trapezoid, upside-down trapezoid, triangle, rectangle with a curved bottom wall, and semicircle are compared. The 0.5 aspect ratio rectangle yields the longest detachment time and the largest detachment diameter, whereas the longest removal time occurs for the 0.25 aspect ratio case. With decreasing aspect ratio for the rectangle the pressure drop increases and the coverage ratio decreases. The 0.1 and 2 aspect ratios rectangles have the largest water saturation. For microchannels with different cross-sections, the detachment time, detachment diameter, and removal time of the water droplet are found to be in this order: triangle < trapezoid < rectangle with a curved bottom wall < rectangle < upside-down trapezoid. The friction coefficient increases by a factor of 2–4 in the presence of water. The upside-down trapezoid yields the maximum coverage ratio and water saturation, while the rectangle with a curved bottom wall results in the minimum values.

1. Introduction

Low-temperature fuel cells, such as polymer electrolyte membrane fuel cells (PEMFCs) and direct methanol fuel cells (DMFCs), have similar membrane electrode assembly (MEA) materials and structure. The MEA is sandwiched between two bipolar plates, which have machined channels for distributing fuel (hydrogen and aqueous methanol solution for PEMFC and DMFC, respectively) and oxidant (mostly oxygen from air). The porous electrodes, commonly referred to as gas diffusion layers (GDLs), are typically made of a regular or random matrix of carbon fibres (carbon cloth or carbon paper). At the cathode side of a PEMFC or DMFC, oxygen diffuses through the GDL and reacts with protons and electrons to produce water. Since these fuel cells are operated at fairly low temperature (below 100 °C), the product water in the gas channels tends to be in liquid form. The formation, phase change, and transport of water have a major impact on the operation, performance, and durability of fuel cells. Water management therefore has been the centre of many papers in the past decade on low-temperature fuel cells ([1,2] among many others). Since liquid water shares the same flow passages with gas reactants, when liquid water is not removed from the cell at a sufficient rate, the transport of reactants is hin-

dered and the so-called flooding may occur as a result. Flooding in a low-temperature fuel cell occurs over a wide range of length scale, i.e. in the meso-pores of the catalyst layer, micro-pores of the GDL and sub-millimeter gas channels. The heterogeneous wettability of the surfaces forming the microchannels, combined with the small hydraulic diameter (ca. 500 µm) and low gas velocity (Reynolds number of order 10^3 or less), yield two-phase flow regimes quite different from those in more conventional engineering applications (e.g. [3,4]).

From fuel cell design standpoint, two key considerations on the water transport in the gas channel are: (1) the dynamics of liquid water droplets, including the detachment process, the ensuing entrainment, and interaction with the channel walls and other droplets and (2) correlation of pressure drop as a function of two-phase flow regimes and operating conditions. On the other hand, the bipolar plate, which accounts for more than 60% of the weight and 30% of the total cost in a typical, graphite-based fuel cell stack [5], is a vital component of fuel cells because it functions as an electron and heat conductor as well as provides flow passages for fuel, oxidant and product water, and provides mechanical support for the unit cells in the stack. The geometry and topology of the gas channels therefore affect the weight, cost and mechanical strength of the bipolar plates. All these factors will ultimately affect the power density of a stack. The topologies of the bipolar plates can include straight, serpentine, or interdigitated flow fields, internal manifolding, internal humidification, and integrated cooling [5].

---

* Corresponding author. Tel.: +86 23 65102474; fax: +86 23 65102474.
E-mail address: zhuxun@cqu.edu.cn (X. Zhu).

The fluid flow channels are typically rectangular in cross-section, even though other configurations such as trapezoidal, triangular, semi-circular, etc. have been explored [6].

In the literature, investigations of the effect of rectangular channel dimensions on cell performances have been reported by some researchers [7–9]. Few researchers reported the effect of channel shape on the cell performance, e.g. [10], where it was shown that triangular and hemispherical shaped cross-section resulted in increase in hydrogen consumption by around 9% at the anode, and consequently, use of such channel would lead to improvement of fuel cell efficiency. However, none of them reported the effects of channel geometry on the dynamics of water droplet subjected to air stream in a microchannel, which is the motivation of the present study.

Many modelling works on water transport for PEMFCs to date have focused on the issues of water flow in the porous components of the cell, e.g. water in the form of saturation in porous media driven by capillary pressure [11–17] and water in the form of absorbed water in the ionomer phase [18–20]. The transport equations derived for these models assumed that water appears as a homogeneous phase within the representative volume. Such an assumption does not extend to liquid water moving in the gas channel due to the presence of large liquid interfaces as a result of interactions between surface tension and the channel walls. Analyses focused on stability and water motion have been reported by Chen et al. [21], Jiao et al. [22] and Quan et al. [23]. These numerical studies considered water droplets as either suspended in the channel, or attached to the channel wall, or a water film on the channel wall without taking into account the process of emergence of liquid water from the GDL into the gas channel. Recently Theodorakakos et al. [24] reported on a thorough investigation on the dynamics of water droplets in a microchannel based on PEMFC by experiments and three-dimensional simulations based on the volume-of-fluid (VOF) methodology. In their work the process was initiated assuming the presence of spherical droplets on the surface without accounting for the emergence process from a pore. The VOF method was also adopted by Zhu et al. in two-dimensional simulations [25,26]. A key aspect of both works was the consideration of flow emerging from a GDL pore and tracking of liquid water emergence into the channel. It was found that accounting for the initial connection of a droplet to a pore yield significantly different dynamics as well as the critical air velocity. While these simulations have provided some valuable, qualitative insights, a complete representation of the dynamic processes requires three-dimensional simulations, cf. [27]. In [27], the authors reported on the physical mechanism of a water droplet emerging from a GDL pore, and an analysis of the growth, deformation, detachment, motion, coalescence and film formation and the associated water coverage and friction factors as a function of operation parameters and surface parameters.

In the present work, the work in [27] is extended to systematically investigate the effect of channel geometry on the dynamic behavior of an emerging water droplet, and to analyze the impact on pressure drop, water saturation, and coverage ratio. The remainder of this paper is organized as follows. The numerical model and the VOF method are briefly outlined, followed by a description of the geometry, physical problem and boundary conditions of the cases considered. Simulation results for different cross-sections of gas channels are then presented, analyzed and compared, closing with and overall assessment of the various channel geometries.

2. Numerical model and VOF method

The VOF method used in this study was initially developed in the 1980s [28], and has been adopted in a number direct numerical simulations of time-dependent flows with multiple, immiscible liquids.

In VOF method, the position of the interface between the fluids of interest is determined by applying a surface-tracking technique to a fixed Eulerian mesh, which is advantageous over methods such as lattice Boltzmann method (LBM), e.g. [29], or boundary integral method [30], because it can be readily integrated into existing computational fluid dynamics (CFD) framework. A volume fraction indicator is used to determine the location of the interfaces of different phases in all cells of the computational domain [28], and a surface reconstruction scheme is then utilized to determine the shape of the interface [31]. The VOF method also allows for modelling of surface force based on the continuum force approach, making it possible to capture surface tension effects.

2.1. Numerical method

Unsteady, isothermal laminar flow conditions are assumed to prevail for both air flow and water droplet motion inside the microchannel, since the bulk flow Reynolds number is less than 170 in the present study and the heat generation and heat transfer are negligible. The three-dimensional numerical model was implemented using the commercial CFD package, FLUENT 6.3.26, and the volume-of-fluid (VOF) method was employed in conjunction with an interface reconstruction algorithm to track the dynamics of the deforming water droplets [32]. More details about the VOF method have been described in reference [27].

2.2. Simulation domain and mesh

A microchannel with square cross-section 250 μm wide and 1000 μm long and a pore of diameter $D = 50$ μm on the GDL surface is chosen as the baseline case in this study. Fig. 1 shows a schematic illustration of the computation domain and the corresponding mesh for the baseline case. These dimensions are representative of gas flow channels used in PEMFCs/DMFCs, and the pore size considered is typical of mean hydraulic diameter values observed in microscope images of GDL [33]. The fixed location of the GDL pore is consistent with experimental observation that indicates water usually appears preferentially on certain site of the GDL surface [33]. In the present model, air flow enters the channel with a velocity U, and water enters the channel through the pore on the GDL surface with a velocity V. This scenario is an idealized representation simulating the emergence into the channel of water produced by electrochemical reaction on the catalyst sites and transported through the GDL. A structured orthogonal computational mesh with 62,835 cells is used for the baseline case. The grid dependency was tested by increasing and decreasing the number of grid nodes by 20% and 40% for the baseline case, and similar water droplet
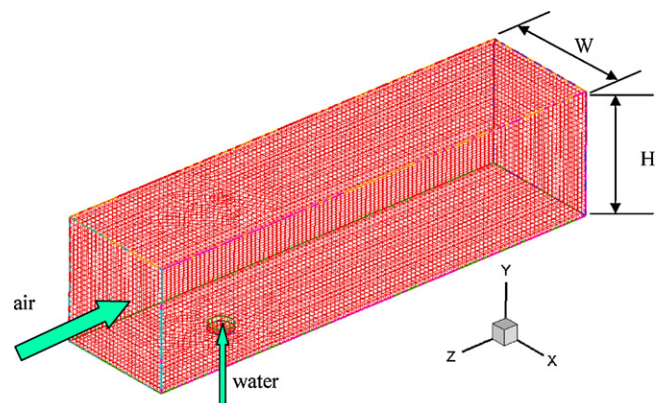

Fig. 1. Computation domain and mesh for the three-dimensional simulations of the baseline case.

Table 1
Parameters for the channel geometry.

Channel geometry	Height (mm)	Width (mm)	Hydraulic diameter (mm)	Area (mm²)	Reynolds number
Rectangle (H/W = 1), baseline	0.25	0.25	0.25	0.0625	157.3
Rectangle (H/W = 2)	0.354	0.177	0.236	0.0625	148.5
Rectangle (H/W = 0.5)	0.177	0.354	0.236	0.0625	148.5
Rectangle (H/W = 0.25)	0.125	0.5	0.2	0.0625	125.8
Rectangle (H/W = 0.1)	0.079	0.79	0.144	0.0625	90.4
Baseline with a curved bottom wall	0.25	0.25	0.209	0.05358	142.8
Trapezoid (H/W = 1)	0.25	0.25	0.207	0.04575	141.8
Upside-down trapezoid (H/W = 1)	0.25	0.25	0.207	0.04575	141.8
Triangle (H/W = 1)	0.25	0.25	0.155	0.03125	105.8
Semicircle (H/W = 0.5)	0.20	0.40	0.244	0.0625	167.3

transport and deformation processes were obtained with all three grids. Therefore the mesh used in the simulation is considered adequate. Preliminary simulations were performed with time steps of 10^{-6}, 10^{-7} and 10^{-8} s, all yielding similar results, and all simulations were consequently performed using a time step of 10^{-7} s.

In order to study the effects of cathode channel geometry on the dynamic behavior of a growing water droplet, several channel cross-sections including rectangle with different aspect ratios, trapezoid, upside-down trapezoid, triangle, rectangle with a curved bottom wall, and semicircle microchannel, are built as the computation domains to compare with the baseline case. The dimensions assigned to the trapezoid, triangle, and rectangle with a curved bottom wall channels are based on the same channel height and width, which is for the practical condition of a given bipolar plate, and the dimensions assigned to the rectangle of various aspect ratios and the semicircle case are of the same area corresponding to the same Re member for air flow. The dimensions of the channel geometries considered in the present study are summarized in Table 1.

2.3. Boundary and initial conditions

All VOF simulations performed in the present study employed uniform velocity profiles for the incoming air in channel and water from the pore, cf. Fig. 1. A convective outflow condition is used at the outlet. No-slip boundary condition is imposed on the walls of the channel and the water pore. Constant surface tension and static contact angle are specified on the wall as a boundary condition. The static contact angle of the bottom wall is set to 140° for all cases, which is based on the typical Teflon treatment for GDL of carbon paper or carbon cloth. The contact angle of all other side walls of the microchannel is 45° for all cases. The simulations start with initial condition of uniform air velocity with no liquid water in the channel.

For all simulations performed, an air velocity of 10 ms^{-1} at a pressure of 1 bar and temperature of 298 K is used. The corresponding Reynolds numbers for air flow, Re$_a$, range from 105 to 170 based on the hydraulic diameter of the channels. Water is injected at 1 ms^{-1} and the corresponding Reynolds number for water injection, Re$_w$, is 50 based on the pore diameter. This velocity value is of similar order of magnitude as those used in ex-situ fuel cell experiments, which corresponds to a fuel cell operation under high current density and water production rates [34,35].

3. Results and discussion

In the following discussion, a series of computational results for the dynamic behaviors of a water droplet in the microchannels with different cross-sections or aspect ratios are shown first, followed by analysis on the observations of these simulations. The geometry considered includes rectangle and rectangle with a curved wall, trapezoid and upside-down trapezoid, triangle and semicircle. Channels with rectangular cross-section are easy to machine

and are the most common geometry. The case of rectangle with a curved wall is in fact a rectangular channel with the intrusion of GDL material into the channel due to compression. The width of the channel determines the opening for water flow out of the GDL and oxygen into the GDL. For a limited design space, the channel width will inherently affect the width of the land where the bipolar plate is in contact with the GDL, which effectively affects electron and heat conduction between the MEA and the bipolar plate. The channel height, on the other hand, will determine the thickness of the bipolar plate, which in turn affects the mechanical strength. Aside from these *static* effects, channel geometry may affect the dynamics of fuel cell operation because of the interactions of liquid water with channel walls. In this paper we focus on the impact on the dynamic behavior of water due to channel geometry.

3.1. Rectangular microchannel

Fig. 2 shows the time evolution of water droplet interface for the baseline case, which is a square channel cross-section, i.e., unity aspect ratio. Because of the hydrophobic bottom wall, water emerges from the pore into the gas channel and forms a droplet (t = 0.6 ms). Surface tension dominates over other forces and keeps the shape of the water droplet fairly spherical at this moment. As time progresses, the water droplet grows larger gradually and nearly blocks the channel. Meanwhile the increasing shear stress and pressure difference between both sides of the water droplet, due to increasing air velocity through the blocked channel, overwhelm surface tension and viscous resistance and remove the water droplet downstream quickly. This makes the upcoming water unable to follow the motion of the main body of the water droplet, leading to a narrow neck (t = 1.3 ms). Then the water droplet breaks up and detaches from the neck at t = 1.4 ms, and moves rapidly to leave the domain (t = 1.6 ms).

Figs. 3–6 show the time evolution of water movement for rectangular channels with different aspect ratios. The cross-section area of these cases is kept the same as the baseline case. In Fig. 3 (aspect ratio = 2), one can see that a water droplet emerges and grows similarly to the baseline case at early time (t = 1.0 ms). However, because of the narrower channel width for this case, the growing water droplet attaches to one side wall (t = 1.2 ms), and soon the attached water droplet quickly spreads on the hydrophilic side wall and detaches from the origin due to surface tension (t = 1.4 ms). The spreading water film and the second emerging water droplet make the air path flexuous, resulting in a complicated pressure profile. Along with the water film being pushed further downstream by air flow, the air flowing around the protuberant water film on the side wall causes a static pressure difference, which then moves the water film upwards to touch the hydrophilic top wall (t = 2.0 ms). This is a phenomenon similar to the so-called Coandă effect. Then part of the water film leaves the computational domain, and the remainder of it remains in the channel due to the corner effect. It is noted that in the next cycle water grows and
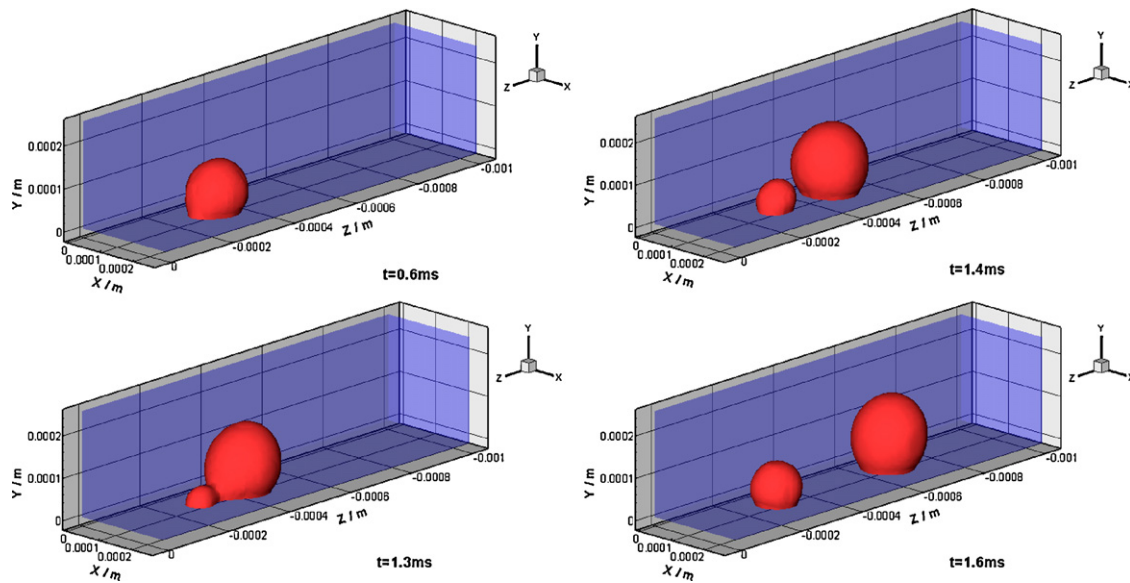
Fig. 2. Time evolution of the dynamic behavior of water droplet in a rectangular microchannel with aspect ratio 1.0.
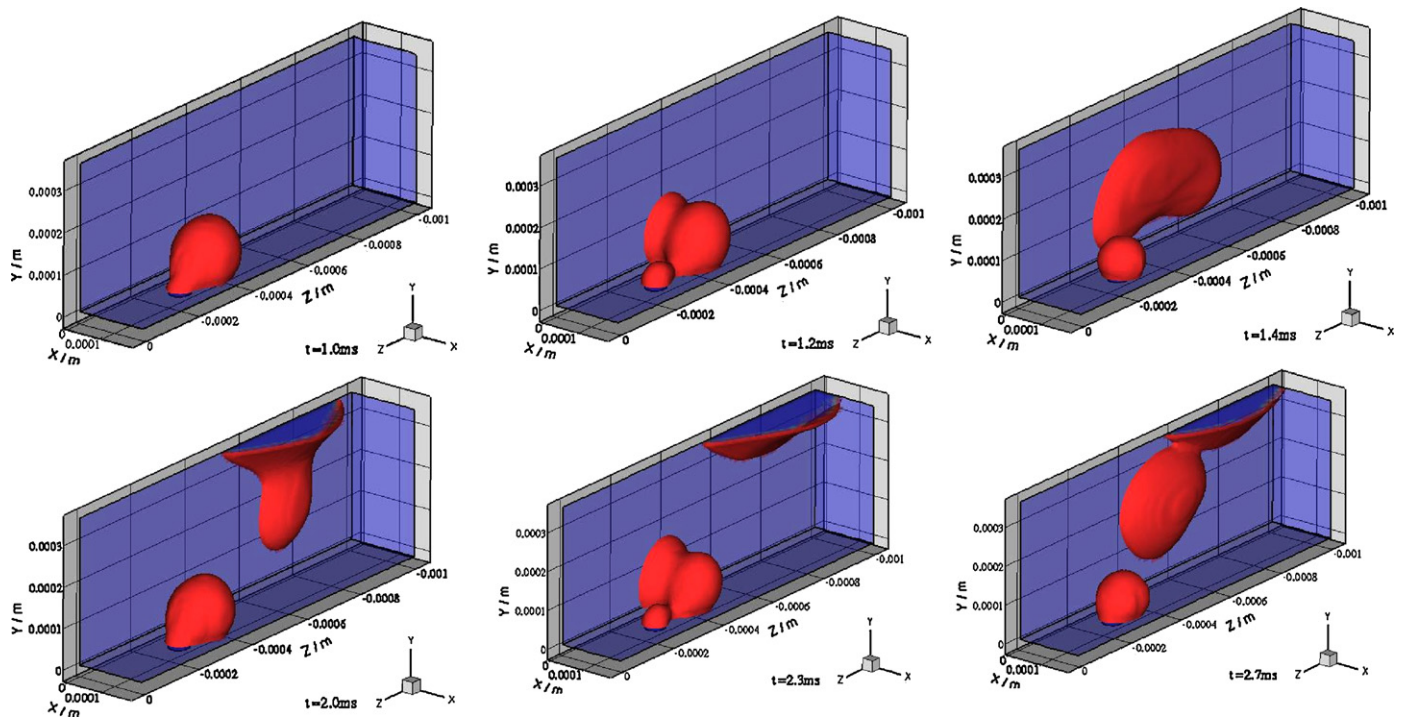

Fig. 3. Time evolution of the dynamic behavior of water droplet in a rectangular microchannel with aspect ratio 2.0.

attaches to the side wall again (t = 2.3 ms). Water movement similar to the first cycle occurs again, and the rising water film from the origin later reaches the remaining water film at the top corner near the channel outlet (t = 2.7 ms). The remaining water in the channel corner appears to become larger, leading to an increase of pressure drop with time.

The time evolution of the water droplet in Fig. 4 (aspect ratio 0.5) shows that the dynamic behaviors of the emerging water droplet are very much similar to those observed in the baseline case. This can be attributed to the movement of isolated water droplet without any effects from the side/top walls. As the aspect ratio is further reduced to 0.25, cf. Fig. 5, the effect of the hydrophilic top wall becomes obvious. Since the height of the channel in this case is

much lower than previous cases, there is no sufficient room for the water droplet to grow to be as large as the baseline case. The water droplet touches the top wall at an early time (t = 0.8 ms), and once this occurs, the water droplet quickly adheres to the hydrophilic top wall and forms a water film due to surface tension, leaving a mushroom neck shape near the pore (t = 1.0 ms). Then the water film retracts due to the principle of minimum interfacial free energy and is pushed downstream by the air flow. This leads to the detachment of the water film from the mushroom neck (t = 1.14 ms). The detached water film flows downstream, and the same behaviors repeat for the second water droplet (t = 2.2 ms). For a even lower aspect ratio, cf. Fig. 6 for aspect ratio 0.1, the water droplet touches the top wall earlier (t = 0.2 ms) than the previous case. A spreading
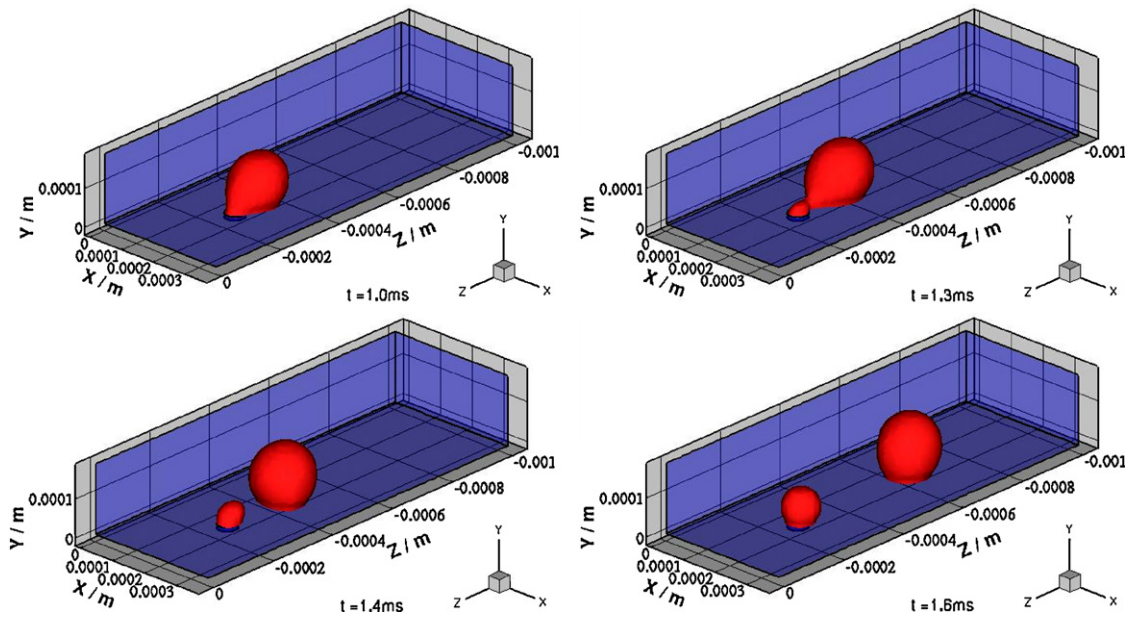
Fig. 4. Time evolution of the dynamic behavior of water droplet in a rectangular microchannel with aspect ratio 0.5.
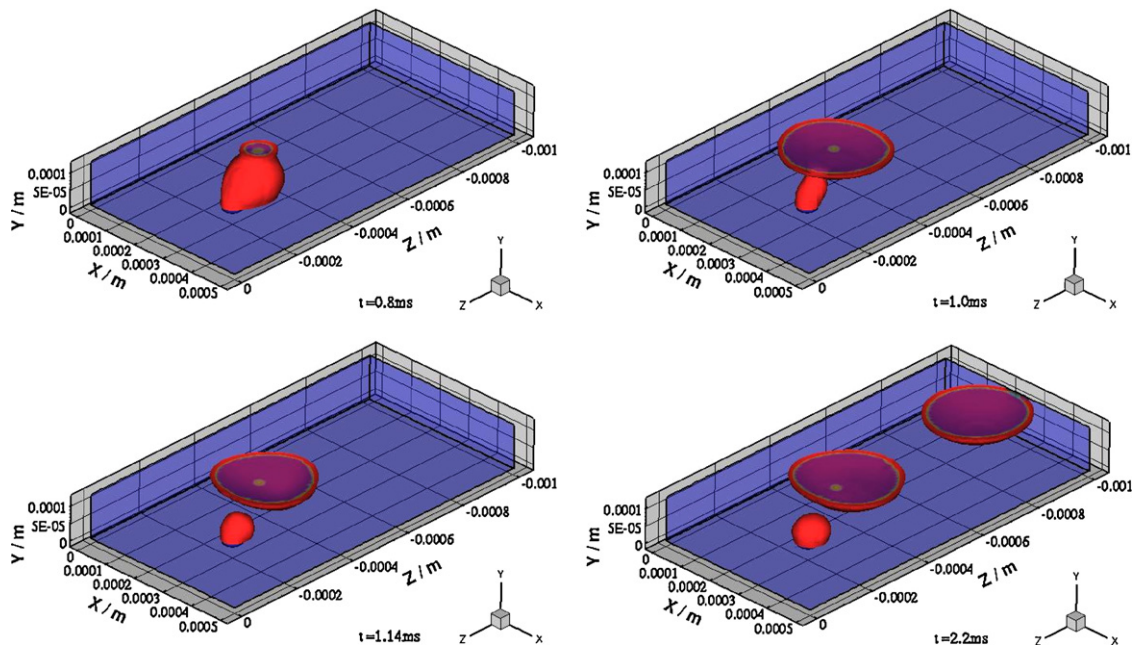

Fig. 5. Time evolution of the dynamic behavior of water droplet in a rectangular microchannel with aspect ratio 0.25.

water film forms on the hydrophilic top wall and a mushroom neck similar to the aspect ratio 0.25 case appears ($t = 1.0$ ms). However, because in this case the spreading rate of water film driven by surface tension and static pressure difference is lower than the water supply from the pore, a continuous water film flow, rather than water detachment as show in Fig. 5, forms from the mushroom neck ($t = 2.0$ ms). Thus, a long stream of film flow carries the water from the pore to leave the channel as time progresses ($t = 3.0$ ms). The implication of this phenomenon is that water is directed away from the bottom GDL surface of the channel and blockage on the GDL surface by water is thus minimized.

Removal of water from its origin and minimum overall pressure drop in the channel are two goals from fuel call design standpoint for channel geometry. Table 2 shows a comparison of the detachment time, detachment diameter, and removal time for the rectangular cases. These parameters characterize the capability of water removal of a microchannel. The detachment time is measured from $t = 0$ to the moment the water droplet breaks up with the original stream. The detachment diameter is the equivalent

Table 2
Detachment diameter, detachment time, and removal time for rectangular channels.

Channel geometry	Detachment time (ms)	Detachment diameter (mm)	Removal time (ms)
Rectangle ($H/W = 2$)	1.22	0.161	2.10[a]
Rectangle ($H/W = 1$)	1.35	0.167	1.90
Rectangle ($H/W = 0.5$)	1.38	0.168	1.90
Rectangle ($H/W = 0.25$)	1.13	0.156	2.68
Rectangle ($H/W = 0.1$)	–	–	2.40[a]

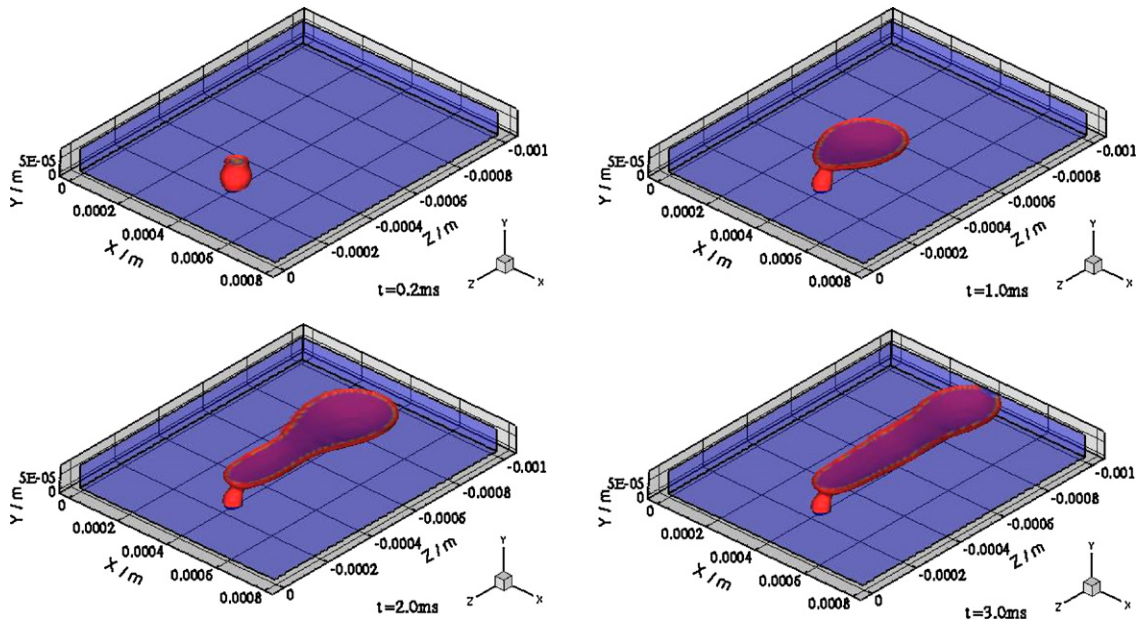[a] Time for the attached water film beginning to move out of the channel.

Fig. 6. Time evolution of the dynamic behavior of water droplet in a rectangular microchannel with aspect ratio 0.1.
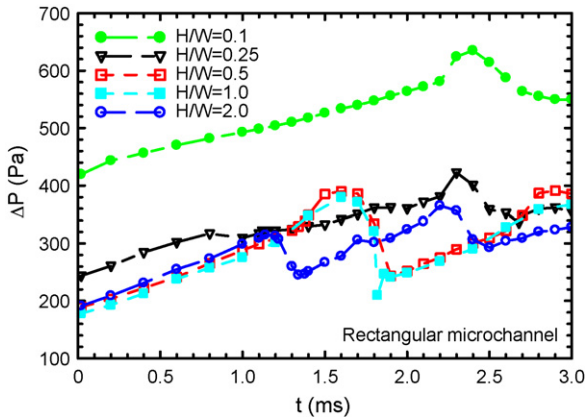

Fig. 7. Time variation of pressure drop for rectangular channels of different aspect ratio.

Fig. 8. Time variation of coverage ratio for rectangular channels of different aspect ratio.

diameter of the volume of detached water droplet. The removal time is defined as the time when the detached water droplet leaves the channel outlet completely. The detachment time is primarily a measure of the effect of the side/top walls as can be seen in the previous discussion, which shows that because spreading of water takes places as soon as its front touches the hydrophilic wall and this spreading tends to lead to detachment of water from its origin. The case of aspect ration 0.5 is found to have the longest detachment time, hence the largest detachment diameter. The longest removal time, on the other hand, occurs in the case with aspect ratio 0.25. The pressure drop between channel inlet and outlet, ΔP, is shown in Fig. 7 for different channel aspect ratios. The pressure drop is very similar for the cases of aspect ratio 1.0 and 0.5 during the same time period. The pressure drop for aspect ratio 0.1 case is the highest at all time because it has the smallest hydraulic diameter among all and also due to the increasing water film thickness on the top wall that blocks the air path. It is noted that the pressure drop for the cases with aspect ratio 2.0 and 0.25 are higher than that of the baseline case during most of the time due to the water that remains at the corner on the top wall.

The GDL surface coverage ratio and water saturation for channels with different aspect ratios are shown in Figs. 8 and 9. The
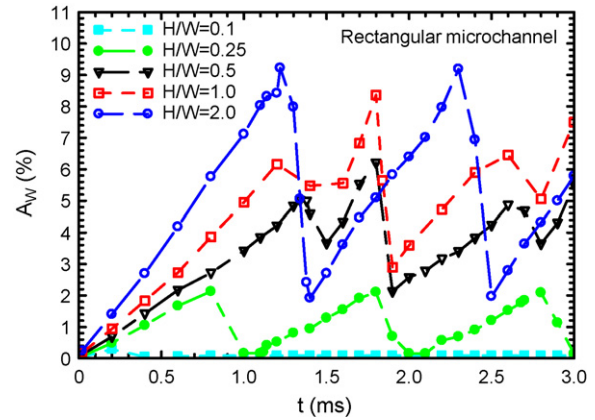
surface coverage ratio A_w is defined as the ratio of the water area on the bottom wall to the area of the bottom wall. The surface ratio is a measure of the impact of liquid water may have on the mass transport between the channel and the GDL. The channel water
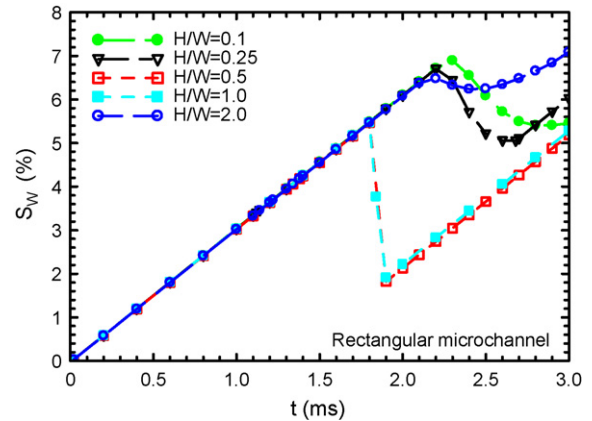

Fig. 9. Time variation of water saturation for rectangular channels of different aspect ratio.
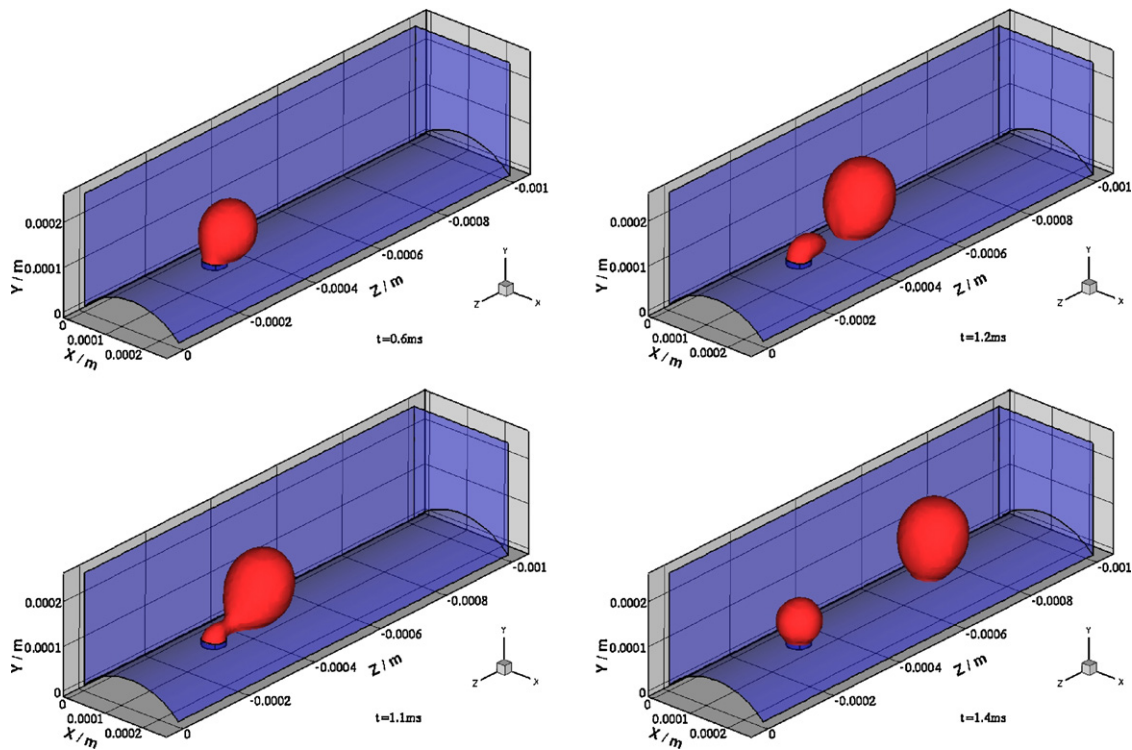
Fig. 10. Time evolution of the dynamic behavior of water droplet in a rectangular microchannel with a curved bottom wall.

saturation S_w is defined as the ratio of the water volume to the channel volume and is an indirect measure of water on pressure drop. From Fig. 8 one can see that the coverage ratio increases with increasing aspect ratio before the water droplet attaches to side/top walls. The coverage ratio reaches a maximum value for the case with aspect ratio 2.0 at early time while it drops significantly once the water droplet attaches to the hydrophilic side wall. Similarly, the coverage ratio drops once the water droplet attaches to the hydrophilic top wall for the case with aspect ratio 0.25. However, for aspect ratios 1.0 and 0.5, the coverage ratio increases till the detached water droplet leaves the channel, followed by a slight decrease in the middle due to the retraction of the triple-phase contact line of the detached water droplet. It is noted that the coverage ratio is near zero for aspect ratio 0.1 due to water attachment to the top wall most of the time. The coverage ratios show a periodic change with the water droplet attaching to side/top walls or flowing out of the channels. The water saturation first increases and then decreases with time when the detached water starts to leave the channel. The longest removal time for the case with aspect ration 0.25 leads to larger water saturation. For aspect ratios 0.1 and 2.0, the resident water in the channel results in the largest saturation. It is noted that for aspect ratios 0.5 and 1, the change of S_w is abrupt because water droplet in both cases is carried away by a high pressure drag due to the form of water as a spherical droplet as opposed to a film for other cases.

3.1.1. Rectangular microchannel with curved bottom wall

When a fuel cell is assembled, the compression force exerted on the bipolar plates may cause deformation of the GDL. The GDL material underneath the land is compressed while that functioning as a wall of the channel is likely to intrude into the gas channel, and therefore modify the channel cross-section. It should be pointed out that GDL intrusion into the channel can be expected in most channel geometries when a fuel cell is assembled. For the sake of simplicity, a rectangular channel is chosen in the present study as an example to show the effect of GDL deformation on water behavior in the

channel. Fig. 10 shows the dynamics of the water droplet in the rectangular microchannel with a curved bottom wall which mimics the situation of intrusion of GDL material into the channel. The height of the curved wall in this case is 51.78 μm, which is 21% of the width of the rectangle. The pore where water is injected from is located on the center line of the curved wall. Compared with the baseline case, the emerging water droplet within the same growing time has less area of solid/liquid interface as well as shorter triple-phase contact line due to the curved wall ($t = 0.6$ ms). As a result, a significant deformation and a fast motion of the droplet body dominated by shear stress and pressure force takes place easily and early, and a longer narrow neck is formed ($t = 1.1$ ms). Then detachment of water droplet occurs ($t = 1.2$ ms) and the detached water droplet, which has a footprint on the curved bottom wall smaller than the baseline, moves out of the channel quickly with the air flow ($t = 1.4$ ms).

3.2. Trapezoidal microchannel

Fig. 11 shows the time evolution of the water droplet in a trapezoidal microchannel. The emergence and formation of the water droplet coming from the pore is similar to those observed in the baseline case at early time ($t = 0.6$ ms). Also the air flow in the microchannel is blocked by the growing water droplet as time progresses. However, the passage between the water droplet and the top wall of the trapezoid is narrower than that in the rectangle and this results in a higher air velocity around the water droplet, hence a stronger shear stress and pressure force on the interface of the water droplet dominating the droplet motion. As a result, the water droplet is pushed quickly downstream and a narrow neck is formed ($t = 1.1$ ms), followed by the earlier detachment of the water droplet from the pore ($t = 1.2$ ms).

3.2.1. Upside-down trapezoidal microchannel

Although not easily to be fabricated in practical bipolar plate manufacturing, an upside-down trapezoidal is of interest to be
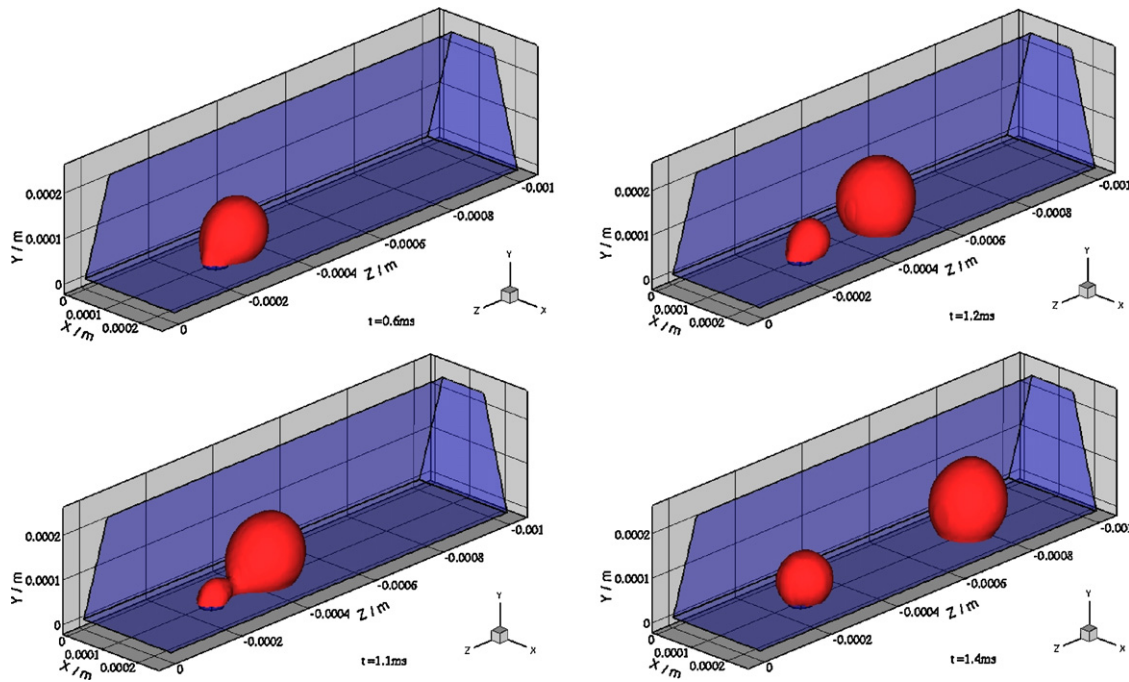
Fig. 11. Time evolution of the dynamic behavior of water droplet in a trapezoidal microchannel.

included in the simulation for comparison purposes. Fig. 12 shows the time evolution of a water droplet in an upside-down trapezoidal microchannel. The results show a completely different dynamic behavior of the water droplet compared to the baseline case and the trapezoid case above. The emerging water droplet grows higher in the upside-down trapezoidal microchannel within the same growth time ($t = 0.6$ ms), which is primarily due to the limitation of the narrow bottom of the trapezoid. However, as time progresses, the water droplet grows to reach the side walls. It is then dragged up to the side walls quickly by surface tension on the triple-phase contact line ($t = 1.0$ ms). Meanwhile, a concave gas/liquid interface is formed at the corners of the side walls and the bottom wall, which induces a surface tension gradient between the center and the corner of the channel. This gradient drives water from the center to the side, and the liquid downstream on the bottom wall retracts, based on the rule of mass conservation, resulting in a saddle shape interface. Thus the bottom wall is covered by the liquid and the spreading water droplet almost blocks the lower half channel ($t = 1$ ms). Furthermore, the water film keeps growing higher due to the constant injection water velocity and blocks more area of the channel. Then the blocked microchannel induces increasing air flow velocity, hence increasing shear stress exerted on the surface of the water film. This pushes the water film on the bottom wall and both the side walls to move downstream to channel outlet. It is noted that a raised head of water droplet is shown at the pore due to continuously entering water and a narrow neck appears because of the motion of the body of the water film ($t = 2.2$ ms). Following this, further increasing shear stress and pressure force resulted from higher air velocity passing through the blocked channel overcome the surface tension to induce the detachment of the water film from the head of the incoming water ($t = 2.3$ ms). The detached water film then moves downstream and a new water droplet forms again ($t = 2.4$ ms). It is noted that a periodic motion occurs after this time, i.e., the water droplet grows to attach to the hydrophilic side walls and a saddle shape interface is formed again accompanying with the removal of the former water film to the outlet of the microchannel ($t = 2.8$ ms). One can see that

the hydrophilic side walls have significant impact to the dynamic behaviors of the water droplet in the upside-down trapezoidal microchannel.

3.3. Triangular microchannel

Fig. 13 shows the dynamics of the water droplet in a triangular microchannel. The simulation results reveal similar dynamic behaviors of the water droplet to those in the baseline case and trapezoid case, including emergence, growth, motion, and detachment because that droplet encounters no effects from the hydrophilic side walls. However, the process of deformation, detachment, and removal of the water droplet is faster than the baseline case. This can be explained by the different velocity profile in the triangle case, which has the same width and height and inlet air velocity as the baseline case. The higher center velocity located close to the bottom wall for the triangle case induces a stronger shear stress exerting on the interface of the water droplet, which promotes the deformation ($t = 0.6$ ms) and the formation of a narrow neck due to the motion of the water droplet ($t = 0.8$ ms). As a result, early detachment of the water droplet takes place ($t = 0.9$ ms), and then the detached water droplet flows out of the channel quickly ($t = 1.0$ ms). This time is much shorter than that in the rectangle and the trapezoid cases.

3.4. Semi-circular microchannel

The time evolution of a water droplet in a semi-circular microchannel, cf. Fig. 14, are similar to that in the rectangular channel. A slight difference is noted in that a new water droplet forms at the front of the trail due to the longer trail shrinking back after the first droplet detaches, whereas in the rectangle case the new water droplet forms just at the pore. The detachment time in the semicircle case is longer and the removal time is shorter than the baseline case, i.e., the motion velocity of the detachment water droplet is faster for the semicircle case.
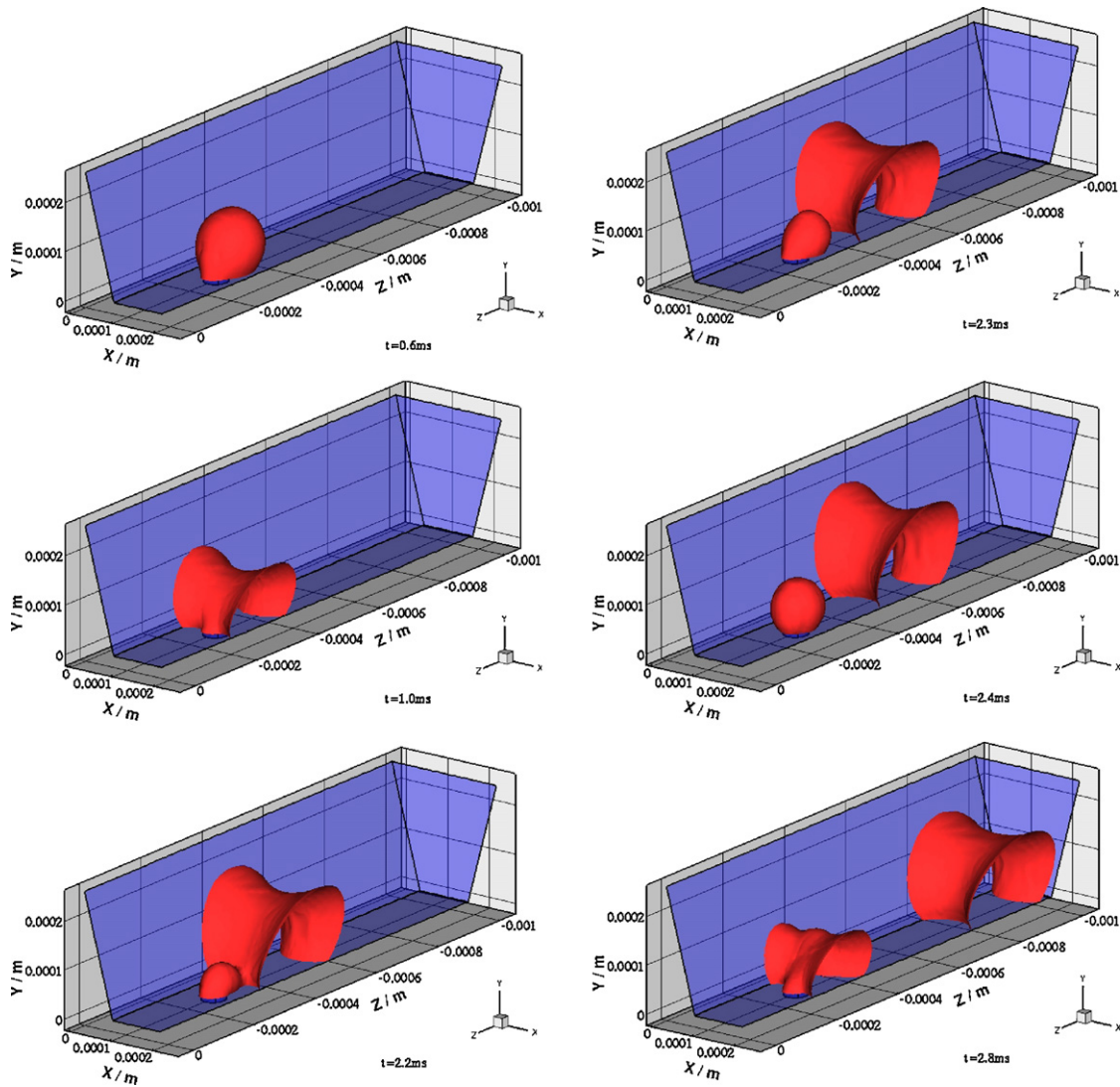
Fig. 12. Time evolution of the dynamic behavior of water droplet in an upside-down trapezoidal microchannel.

3.5. Quantitative comparison of simulation results from different channel geometry

Table 3 shows a comparison of the detachment time, detachment diameter, and removal time of the water droplet in channels of different geometry. For the cases tested, the detachment time, removal time and the detachment diameter are found to be in this order: triangle < trapezoid < rectangle with a curved bottom wall < semicircle < rectangle < upside-down trapezoid, except a slightly different order in the last three for the detachment time, which is rectangle < semicircle < upside-down trapezoid. In addi-

Table 3
Comparison of detachment diameter, detachment time, and removal time for different microchannels.

Channel geometry	Detachment time (ms)	Detachment diameter (mm)	Removal time (ms)
Rectangle	1.35	0.167	1.9
Rectangle with curved bottom wall	1.2	0.160	1.62
Trapezoid	1.16	0.158	1.56
Upside-down trapezoid	2.25	0.199	3.1
Triangle	0.86	0.140	1.16
Semicircle	1.4	0.165	1.88

tion to these quantities related to characteristics of the droplet motion, another important parameter for fuel cell operation is the friction coefficient of the gas flow, which determines the extent of flow maldistribution or non-uniformity induced in a manifold design due to partial flooding of one channel. The time evolution of the flow friction coefficient, defined as [36]

$$f = \frac{\Delta p}{(1/2)\rho u_a^2 (L/D_H)} \tag{1}$$

is shown in Fig. 15, where u_a and ρ are the inlet velocity and density of air respectively, L and D_H are the length and hydraulic diameter of the channel respectively. The dimensionless time, τ, is physical time normalized by the time when the detached water droplet just exits the channel. The *air* flow friction coefficient f_a is the reference flow friction coefficient for air only flow through the channel. The ratio of the *wet* friction coefficient f with respect to the *dry* friction coefficient f_a is a measure to assess the additional pumping requirements due to the presence of liquid water. For all the cases tested, the friction coefficient f increases as time progresses due to increasing water volume blocking air flow, and drops back after the detached droplet moves out of the channel. The smallest increase in the friction coefficient is the semicircle channel, and the upside-down trapezoidal channel achieves the highest relative flow friction coefficient due to the attachment of two water droplets
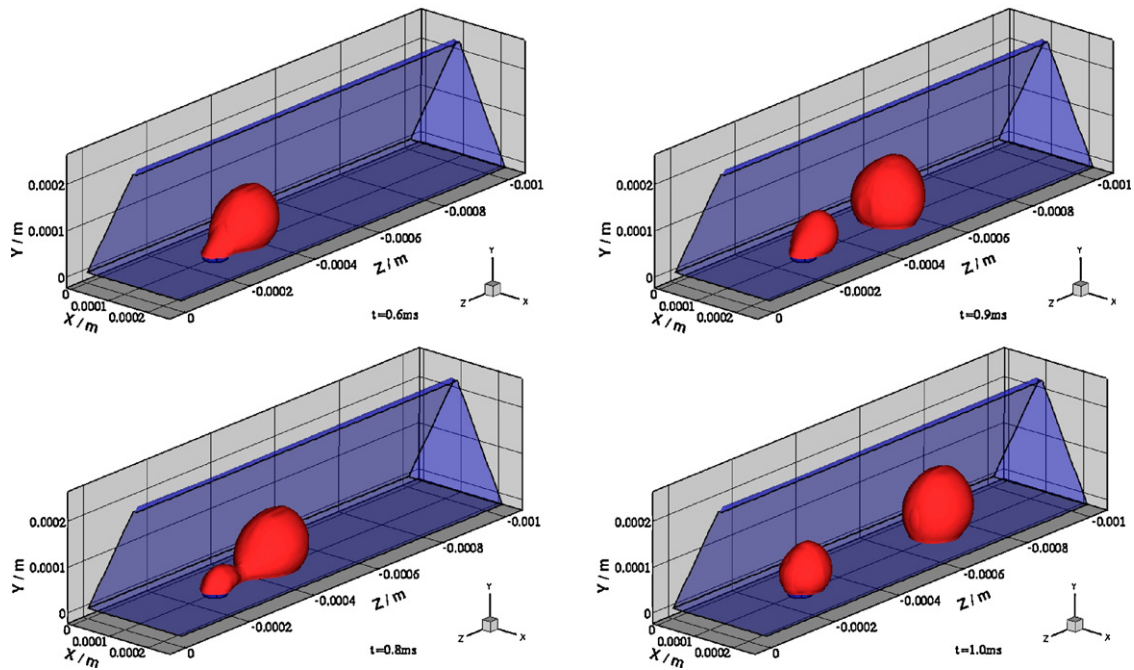
Fig. 13. Time evolution of the dynamic behavior of water droplet in a triangular microchannel.

with side walls that severely blocks the air flow path. The triangular channel has the second highest increase in friction coefficient due to its narrow air path in the upper part of the channel.

The GDL surface coverage ratio and the water saturation for different channel geometries are shown in Figs. 16 and 17. Both water saturation and coverage ratio increase with time due to the continuous inflow of liquid water, and they drop dramatically when water leaves the channel. Both coverage ratio and water saturation sharply increase in the upside-down trapezoidal channel, and has the maximum value among all cases. The rectangular channel with a curved bottom wall has the minimum coverage ratio and water saturation, while diverse differences are seen among all other cases.

It can be expected that the attachment of water droplet to the side walls in the upside-down trapezoidal channel results in high resistance and slow motion of the water. This is proved by the longest detachment time and removal time as well as the largest detachment diameter, cf. Table 3. The slow motion water dragged by the hydrophilic side walls increases the triple-phase contact line of the water, hence the high coverage ratio and water saturation. Indeed, it is also noted that the upside-down trapezoidal channel, in which the top wall has the same width as the rectangular channel, has a minimum area of the bottom wall among all cases, and this should be considered to be one of the reasons for the high coverage ratio. However, for the rectangular channel with a curved bottom wall,
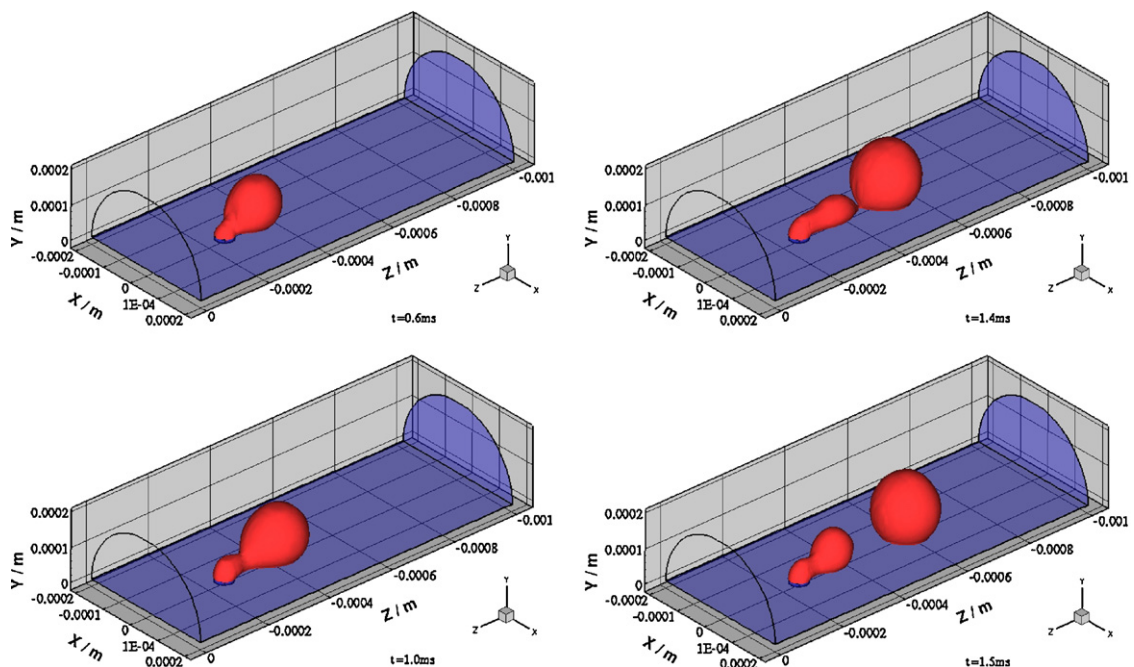

Fig. 14. Time evolution of the dynamic behavior of water droplet in a semicircle microchannel.
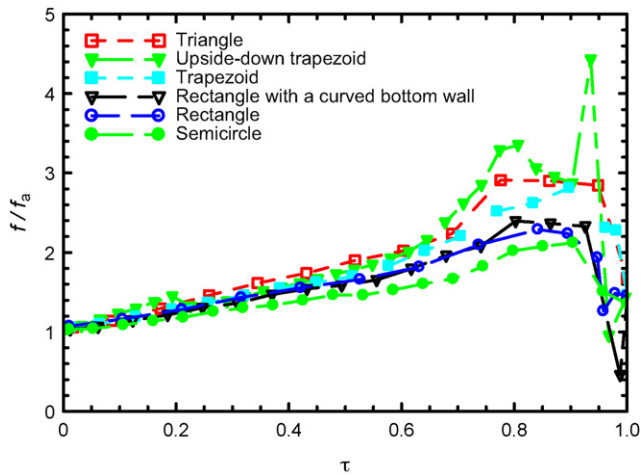
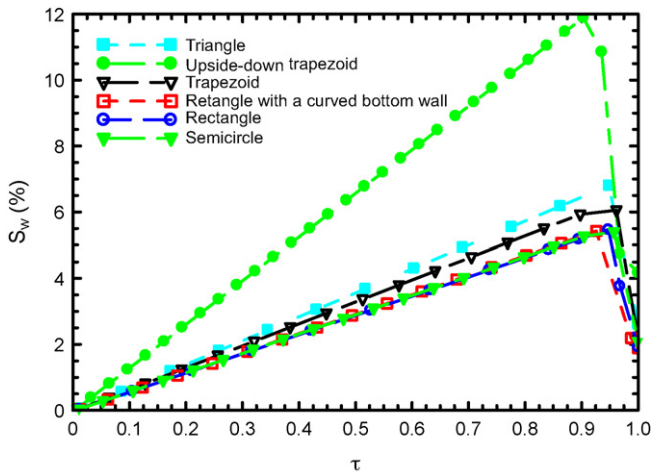**Fig. 15.** Time variation of normalized friction coefficient for channels of different cross-section.

Fig. 16. Time variation of water volume saturation for channels of different cross-section.

water droplet tends to grow upwards on the bottom wall due to the hydrophobic protuberant surface inducing small detachment diameter and short detachment time, hence the low coverage ratio and water saturation.
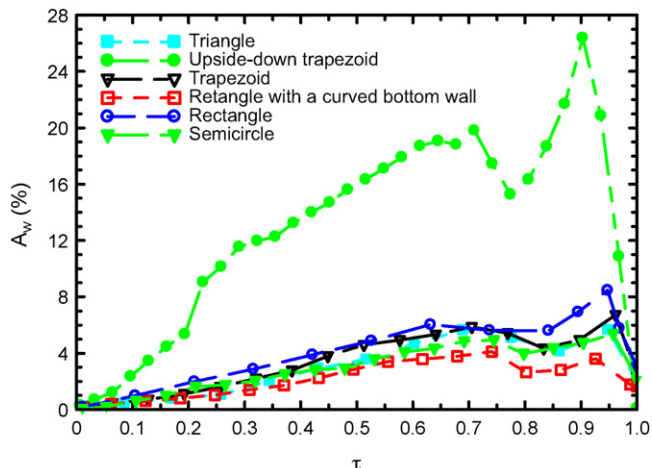

Fig. 17. Time variation of coverage ratio for channels of different cross-section.

In our opinion, the criteria for a good cathode channel include low flow resistance, low water saturation in the channel, and low water coverage on the GDL surface. Based on these criteria and our simulation results, the rectangular microchannel is found to be a good choice among the channel geometries considered. In particular, the rectangular microchannel with an aspect ratio 0.5 is recommended. It should be pointed out that GDL intrusion, the case with a curved bottom wall in the present study, was found to be beneficial for water evacuation as well.

4. Conclusions

The dynamic behaviors of water droplets emerging from a pore into a straight microchannel are simulated using a three-dimensional model in conjunction with the volume-of-fluid (VOF) method. The effects of the channel geometry on the evolution and motion of the water droplets, flow resistance, water saturation and coverage ratio are investigated. The main findings and conclusions of the study are:

(1) The geometry of the microchannel has a significant impact on the dynamic behaviors and on the overall pressure drop. For the wettable configuration (three hydrophilic walls and a hydrophobic bottom wall), the movement of water changes drastically when a droplet surface is in contact with the hydrophilic walls. For a narrow channel (high aspect ratio), this occurs on the side walls first. For a flatter channel (low aspect ratio), this occurs at the top wall first.

(2) For the cases of rectangular channel geometry, the longest detachment time and the largest detachment diameter occur for aspect ratio 0.5, yet the longest removal time occurs for the 0.25 aspect ratio. The pressure drop for the case with aspect ratio of 0.1 is the highest. The coverage ratio initially increases with time as well as aspect ratio. It then drops once the water droplet attaches to the side/top walls and moves out of the channel. The rectangles with aspect ratio of 0.1 and 2.0 overall have the higher water saturation.

(3) For microchannels with different cross-section geometry, the detachment time, detachment diameter, and the removal time of water droplet increase in this sequence: triangle < trapezoid < rectangle with a curved bottom wall < rectangle < upside-down trapezoid. The detachment time for semicircle channel is longer than the rectangle, while its detachment diameter is smaller and the removal time is shorter than the rectangle.

(4) The relative flow friction coefficient varies for different microchannels and the presence of liquid water is found to cause increase of friction coefficient by a factor of 2–4. The upside-down trapezoid achieves the highest relative friction coefficient, followed by the triangle case, whereas the semicircle is the lowest.

(5) Both coverage ratio and water saturation increase sharply in the upside-down trapezoidal channel, and the maximum values occur for this case. For the cases with aspect ratio of H/W around unity, the rectangular channel with a curved bottom wall has the minimum coverage ratio and water saturation, while diverse differences are seen among other cases. The rectangle case with 0.1 aspect ratio has the lowest coverage ratio because most of the water from the GDL pore attaches to the top wall and exits the channel from there, leaving almost no water on the bottom wall.

References

[1] J.J. Kowal, A. Turhan, K. Heller, J. Brenizer, M.M. Mench, J. Electrochem. Soc. 153 (2006) A1971–A1978.
[2] A. Taniguchi, T. Akita, K. Yasuda, Y. Miyazaki, J. Power Sources 130 (2004) 42–49.
[3] K.A. Triplett, S.M. Ghiaasiaan, S.I. Abdel-Khalik, D.L. Sadowski, Int. J. Multiphase Flow 25 (1999) 377–394.
[4] T.A. Trabold, Heat Transfer Eng. 26 (2005) 3–12.
[5] X. Li, I. Sabir, Int. J. Hydrogen Energy 30 (2005) 359–371.
[6] E. Hontanon, M.J. Escudero, C. Bautista, P.L. Garcia-Ybarra, L. Daza, J. Power Sources 86 (2000) 363–368.
[7] J. Scholta, G. Escher, W. Zhang, L. Küppers, L. Jörissen, W. Lehnert, J. Power Sources 155 (2006) 66–71.
[8] J. Scholta, F. Häussler, W. Zhang, L. Küppers, L. Jörissen, W. Lehnert, J. Power Sources 155 (2006) 60–65.
[9] W. Sun, B.A. Peppley, K. Karan, J. Power Sources 144 (2005) 42–53.
[10] A. Kumar, R.G. Reddy, J. Power Sources 113 (2003) 11–18.
[11] Z.H. Wang, C.Y. Wang, K.S. Chen, J. Power Sources 94 (2001) 40–50.
[12] U. Pasaogullari, C.Y. Wang, J. Electrochem. Soc. 151 (2004) A399–A406.
[13] J.J. Baschuk, X.H. Li, J. Power Sources 86 (2000) 181–196.
[14] N.P. Siegel, M.W. Ellis, D.J. Nelson, M.R. von Spakovsky, J. Power Sources 128 (2004) 173–184.
[15] L.X. You, H.T. Liu, Int. J. Heat Mass Transfer 45 (2002) 2277–2287.
[16] M.R. Hu, A.Z. Gu, M.H. Wang, X.J. Zhu, L.J. Yu, Energy Convers. Manage. 45 (2004) 1861–1882.
[17] T. Berning, N. Djilali, J. Electrochem. Soc. 150 (2003) A1589–A1598.
[18] T.E. Springer, T.A. Zawodzinski, S. Gottesfeld, J. Electrochem. Soc. 138 (1991) 2334–2342.
[19] P.C. Sui, N. Djilali, ASME J. Fuel Cell Sci. Technol. 2 (2005) 149–155.
[20] J. Fimrite, H. Struchtrup, N. Djilali, J. Electrochem. Soc. 152 (2005) A1804–A1814.
[21] K.S. Chen, M.A. Hickner, D.R. Noble, Int. J. Energy Res. 29 (2005) 1113–1132.
[22] K. Jiao, B. Zhou, P. Quan, J. Power Sources 157 (2006) 226–243.
[23] P. Quan, B. Zhou, A. Sobiesiak, Z.S. Liu, J. Power Sources 152 (2005) 131–145.
[24] A. Theodorakakos, T. Ous, A. Gavaises, J.M. Nouri, N. Nikolopoulos, H. Yanagihara, J. Colloid Interface Sci. 300 (2006) 673–687.
[25] X. Zhu, P.C. Sui, N. Djilali, J. Power Sources 172 (2007) 287–295.
[26] X. Zhu, P.C. Sui, N. Djilali, Microfluidics Nanofluidics 4 (2008) 543–555.
[27] X. Zhu, P.C. Sui, N. Djilali, J. Power Sources 181 (2008) 101–115.
[28] C.W. Hirt, B.D. Nichols, J. Comp. Phys. 39 (1981) 201–225.
[29] A. Golpaygan, N. Ashgriz, 14th Annual Conference of the Computational Fluid Dynamics of Canada, Kingston, Canada, 2006.
[30] J. Billingham, A.C. King, J. Fluid Mech. 296 (1995) 325–351.
[31] D.L. Youngs, Time-Dependent Multi-Material Flow with Large Fluid Distortion, Academic Press, New York, 1982.
[32] Fluent, Fluent 6.2 User's Guide, 2006.
[33] S. Litster, D. Sinton, N. Djilali, J. Power Sources 154 (2006) 95–105.
[34] A. Bazylak, D. Sinton, Z.S. Liu, N. Djilali, J. Power Sources 163 (2007) 784–792.
[35] E.C. Kumbur, K.V. Sharp, M.M. Mench, J. Power Sources 161 (2006) 333–345.
[36] H. Yamaguchi, Engineering Fluid Mechanics, Springer, Dordrecht, Netherlands, 2008.